Nonequilibrium molecular dynamics methods for computing the thermal conductivity: Application to amorphous polymers

Takamichi Terao,[1,*] Enrico Lussetti,[2] and Florian Müller-Plathe[2]
[1]*Department of Mathematical and Design Engineering, Gifu University, Gifu 501-1193, Japan*
[2]*Eduard-Zintl-Institut für Anorganische und Physikalische Chemie, Technische Universität Darmstadt, Petersenstrasse 20, 64287 Darmstadt, Germany*

(Received 8 November 2006; revised manuscript received 8 March 2007; published 25 May 2007)

We develop two nonequilibrium simulation methods which are suitable for calculation of thermal conductivity with good accuracy. These methods are based on simple algorithms, and it will be very easy to extend their range of application. In particular, there are no restrictions (from, e.g., the force field) to apply them to a variety of systems. Here, they are applied to the calculation of the thermal conductivity of amorphous polyamide-6,6 systems. We treat two models of the polymer with different degrees of freedoms constrained. The results suggest that the methods are quite efficient, and that thermal conductivity strongly depends on the number of degrees of freedom in the model.

DOI: 10.1103/PhysRevE.75.057701 PACS number(s): 02.70.Ns, 61.20.Ja, 82.70.−y

In recent decades, numerical methods for nonequilibrium molecular dynamics (NEMD) have been proposed for studying transport properties of systems, such as the thermal conductivity and the shear viscosity [1–7]. The reverse nonequilibrium molecular dynamics (RNEMD) method in particular has the advantage that total energy and total linear momentum are conserved, and it has been successfully applied to various systems such as Lennard-Jones fluids, molecular liquids and their mixtures, as well as polymer systems [2,4,5,8]. In the RNEMD method, a heat flux through the system is artificially generated by suitably exchanging particle velocities in different regions. The periodic system is divided equally into slabs along one direction, with one of these slabs defined as a "hot slab" and another as a "cold slab." At intervals of several hundred time steps, the center-of-mass Cartesian velocity vectors of the "coldest" particle in the hot slab and the "hottest" particle in the cold one of equal mass are swapped (for details of the method, see Ref. [2]). However, it is difficult to apply the RNEMD method to force fields with all bond distances constrained, since velocity-exchange procedures between different atoms often violate the constraint conditions of the SHAKE method [9]. These problems have been discussed in detail elsewhere [4,5].

To overcome this difficulty, numerical methods especially suited for fully constrained models are proposed here for the calculation of thermal conductivity, termed the *dual-thermostat method and heat-injection method*. Using these numerical algorithms, we can obtain the thermal conductivity of fully constrained polymer systems with high accuracy. Because no assumption is made concerning the details of force fields, these NEMD methods are widely applicable. In this paper, we demonstrate the accuracy and efficiency of these algorithms by examining the thermal conductivity of amorphous polyamide-6,6 (PA66) systems [10].

The thermal conductivity κ is defined by the linear-response relation

$$\boldsymbol{j} = -\kappa \nabla T \tag{1}$$

where ∇T is a temperature gradient and $\boldsymbol{j}$ is a heat flux vector. In the following, we describe the methods for calculating the thermal conductivity κ. The first one is the dual-thermostat (DT) method, with a setup as shown in Fig. 1(a). In this method, slab H and slab C are coupled with Berendsen thermostats locally, and each slab is set to remain at a constant temperature [9]. The temperatures of the thermostated slabs are set to be $T_0=T_H$ for slab H and $T_0=T_C$ for slab C $(T_H>T_C)$; the system reaches a steady state after sufficient time, and a linear temperature profile is obtained in the intervening slabs.

In some of the previous computer simulations of the thermal conductivity, the magnitude of heat flux was numerically obtained by the fluctuation-dissipation theorem [11]. In these methods, the statistical error of the calculated thermal conductivity can become quite large. We employ a different numerical method here: in slab H, the Berendsen thermostat creates energy in the system (on average), while the thermostat in slab C removes energy from the system. We did not perform any temperature control in the intervening unthermostated slabs, so the change in total energy per time step $\langle \Delta E_{total} \rangle$ becomes $\langle \Delta E_{total} \rangle = \langle \Delta E_H \rangle + \langle \Delta E_C \rangle + \langle \Delta E_{err} \rangle$, where $\langle \Delta E_{err} \rangle$ is the change due to numerical errors per MD step, and $\langle \cdots \rangle$ denotes time averaging. After the system reaches a stationary state ($\langle \Delta E_{total} \rangle = 0$), $\langle \Delta E_H \rangle + \langle \Delta E_C \rangle$ must be zero if the integration error can be neglected. In practice, a nonzero value of $\langle \Delta E_H \rangle + \langle \Delta E_C \rangle$ results from the integration error in the simulation, and it shows the accuracy of the calculated thermal conductivity.

In this method, both the energy creation rate and the energy removal rate can be calculated. In each time step, we evaluate the energy changes ΔE_H and ΔE_C due to the Berendsen thermostat coupled with slabs H and C, which are given by $\Delta E_i \equiv (\eta_i^2 - 1) E_i^K$ $(i=H,C)$, where η_i, ΔE_i, and E_i^K are the velocity scaling factor in slab i, the energy change due to velocity scaling by the Berendsen thermostat, and the kinetic energy in the slab i given by $E_i^K = \Sigma_{j \in i} m_j \mathbf{v}_j^2 / 2$, respec-

*Corresponding author.

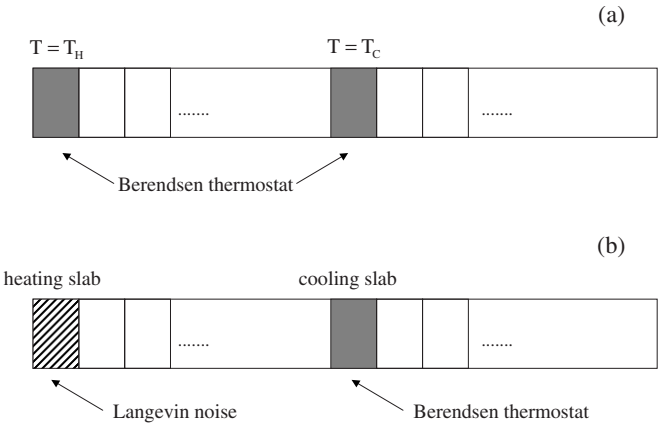

FIG. 1. Schematic view of the numerical methods: (a) the dual-thermostat method and (b) the heat-injection method.

tively. Here, the summation is performed over atoms j contained in slab i. As a result, the thermal conductivity κ is obtained from the above calculations as

$$\kappa = \frac{1}{2S}\frac{\langle|\Delta E_i/\Delta t|\rangle}{\langle|dT(z)/dz|\rangle}, \tag{2}$$

where $\langle\cdots\rangle$ is the time averaging, S is the cross-sectional area of the simulation box perpendicular to flow direction z, and the factor 2 arises from the periodicity.

We also propose an alternative method called the heat-injection (HI) method. The setup of this method is shown in Fig. 1(b). The main difference between the HI method and DT method is the treatment of slab H (hot slab). Using a well-equilibrated sample, slab H is heated by adding a random Langevin-noise term to the equation of motion for each atom j in the slab,

$$m_j\frac{d^2}{dt^2}\mathbf{r}_j(t) = \mathbf{F}_j(t) + \mathbf{W}_j(t), \tag{3}$$

where $\mathbf{W}_j(t) \equiv (W_j^x(t), W_j^y(t), W_j^z(t))$ is a white noise for heat generation. Here $W_j^\alpha(t)$ $(\alpha = x, y, z)$ are Gaussian random numbers with zero mean and variance σ. In addition, slab C is set to remain at a constant temperature by coupling a Berendsen thermostat locally. In this geometry, the heat generated by the Langevin noise (slab H) flows to the heat sink (slab C). After a sufficiently long period of time, the system reaches a steady state with a finite temperature gradient $dT(z)/dz$. Next, we calculate the rate of increase in total energy $\Delta E_{tot}(t)/\Delta t$ with the Berendsen thermostat in slab C turned *off*. In principle, this is equal to the amount of thermal energy added to the system per unit of time, caused by the Langevin noise in slab H.

From these two independent calculations, thermal conductivity κ is obtained as

$$\kappa = \frac{1}{2S}\frac{\langle\Delta E_{tot}(t)/\Delta t\rangle}{\langle|dT(z)/dz|\rangle}. \tag{4}$$

Equations (2) and (4) have the same form, although the physical origin of the numerator in Eqs. (2) and (4) differs; in Eq. (4), $\langle\Delta E_{tot}(t)/\Delta t\rangle$ indicates the strength of the externally injected heat, which is obtained from independent simulation. It should be noted that in both methods, thermostating is limited to the hot and the cold slab. In the intervening slabs, which constitute the majority of the system, where heat conduction takes place, and where the calculation of the temperature gradient is performed, the system follows the pure Newtonian dynamics. It would therefore appear that, first, also other thermostats are permissible with both algorithms and that, second, the use of the sometimes criticized Berendsen thermostat is not critical here.

To check the accuracy of these two numerical methods described above, the thermal conductivity of a monodisperse Lennard-Jones system with reduced temperature $T^*=0.7$ and density $\rho^*=0.85$ is calculated. The reduced thermal conductivity κ^* (in Lennard-Jones units) becomes $\kappa^*=7.1\pm0.4$ for the DT method, and $\kappa^*=6.6\pm0.7$ for the HI method. These results are in good agreement with those of a previous study using RNEMD (6.4–6.9, depending on the conditions) [2].

In the following, we calculate the thermal conductivity of amorphous PA66 systems by the DT method, and demonstrate its efficiency. We study an all-atom model of PA66 with bond constraints (referred to as the AA model), which is described in Ref. [10]. The intramolecular force field contains harmonic bond angle bending and periodic cosine-type torsional potentials. The nonbonded potential includes Lennard-Jones terms, with Lorentz-Berthelot mixing rules, and electrostatic interactions for the models with partial atomic charges. The latter are treated using the reaction-field method, with a dielectric constant of 5. In addition, we also consider a fully bond-constrained united-atom model (referred to as UA model) derived from the AA model, in which all of the CH_2 and CH_3 groups are treated as single atoms and all of the intramolecular bonds are rigid. The Lennard-Jones parameters ε and σ of UA model are given by $\varepsilon=0.48$ kJ/mol and $\sigma=0.393$ nm for CH_2 groups, and $\varepsilon=0.73$ kJ/mol and $\sigma=0.393$ nm for CH_3 groups, respectively. The density is set to 1.11 g/cm^3 for the AA model, and 1.07 g/cm^3 for the UA model. All molecular dynamics simulations are carried out with the YASP package [6]. The equation of motion is solved by a leap-frog algorithm, and bond constraints, if present, are solved by the SHAKE method [9,12]. The simulation cells are elongated in the z direction, and periodic boundary conditions are imposed in all directions.

The system size of the UA model is taken to be L_x, $L_y=5.49$ nm, and $L_z=10.97$ nm, and the total number of (united) atoms is $N=17\,328$. We calculate the energy changes within the two thermostated slabs ΔE_H and ΔE_C at each MD step. To confirm the numerical accuracy of the DT method, calculations are performed with 10^6 MD steps of two different step lengths, $\Delta t=0.5$ fs and 1.0 fs, after the system reaches steady state. The temperatures in the thermostated slabs are set to $T_H=310$ K and $T_C=290$ K, and the coupling time of the local Berendsen thermostat in both slabs is 0.1 ps to keep the average temperature within 0.3 K of the target temperature. The resulting temperature profile is shown in Fig. 2. The energy changes per step due to the

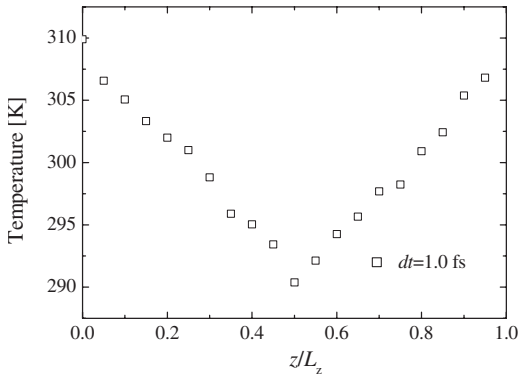

FIG. 2. Temperature profile of the UA model obtained by the dual-thermostat method.

thermostat in each slab become $\langle \Delta E_H \rangle = 3.18 \times 10^{-2}$ kJ/mol and $\langle \Delta E_C \rangle = -3.73 \times 10^{-2}$ kJ/mol with $\Delta t = 1.0$ ps, and $\langle \Delta E_H \rangle = 1.75 \times 10^{-2}$ kJ/mol and $\langle \Delta E_C \rangle = -1.76 \times 10^{-2}$ kJ/mol with $\Delta t = 0.5$ ps. Here, the difference between the energy creation rate $\langle \Delta E_H \rangle$ and the energy removal rate $-\langle \Delta E_C \rangle$ shows the magnitude of integration errors due to the finite time step Δt. This difference becomes smaller with the time step Δt. The convergence of the DT method, with time steps $\Delta t = 1.0$ fs and 0.5 fs, is shown in Fig. 3. The solid and the dashed lines in Fig. 3 show $\langle \Delta E_H \rangle$ and $-\langle \Delta E_C \rangle$, respectively, where the cumulative average of the energy change in the thermostated slab $\langle \Delta E_i \rangle$ $(i = H, C)$ is defined as

$$\langle \Delta E_i \rangle = \frac{1}{t} \int_0^t \Delta E_i(t') dt', \tag{5}$$

where $\Delta E_i(t')$ is the energy change at time t'. The average energy change $\langle \Delta E_i \rangle$ due to the Berendsen thermostat coupled to the slabs is found to converge after $t \geq 4 \times 10^2$ ps. Moreover, the difference between $\langle \Delta E_H \rangle$ and $-\langle \Delta E_C \rangle$ remained constant after this period of time, see Fig. 3(a). As a result, the thermal conductivity of the UA model was $\kappa = 0.27 \pm 0.03$ W m^{-1} K^{-1} for $\Delta t = 1.0$ fs, and $\kappa = 0.27 \pm 0.01$ W m^{-1} K^{-1} for $\Delta t = 0.5$ fs.

We also examine the thermal conductivity of the AA model by the DT method. The system size is L_x, $L_y = 5.46$ nm and $L_z = 10.92$ nm, and the total number of atoms is $N = 36\,720$. Calculations are performed for 10^6 MD steps of length $\Delta t = 0.5$ fs, after the system reached the steady state. With slab temperatures set to $T_H = 310$ K and $T_C = 290$ K, the thermal conductivity in the AA model becomes $\kappa = 0.38 \pm 0.01$ W m^{-1} K^{-1}.

In addition, the thermal conductivity of the fully bond-constrained UA model of amorphous PA66 is calculated by the HI method [Fig. 1(b)], in order to compare the two methods for the same polymer model. First, we calculate the rate of increase of the total energy $\Delta E_{tot}(t)/\Delta t$ for different magnitudes of the Langevin noise term [variance $\sigma = 30.0$, 15.0, and 10.0 in Eq. (3), denoted as cases I, II, and III] with the Berendsen thermostat in slab C turned *off*. The resulting linear increase of the total energy $\langle \Delta E_{tot}(t)/\Delta t \rangle$ is estimated to be 0.14 kJ/mol/fs, 0.042 kJ/mol/fs, and 0.024 kJ/mol/fs

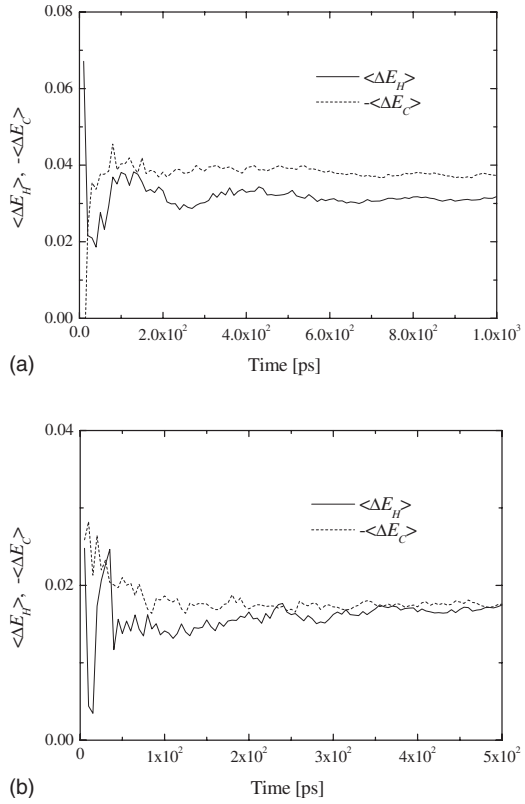

FIG. 3. Dual-thermostat method: Cumulative average of the energy change per time in the thermostated slabs $\langle \Delta E_i \rangle$ $(i = H, C)$ with the UA model. (a) $dt = 1.0$ fs, (b) $dt = 0.5$ fs.

in cases I, II, and III, respectively. Second, the three calculations are repeated with the same settings of the Langevin noise term and with the Berendsen thermostat in the cooling slab turned *on*. From the resulting temperature profiles, the temperature gradients $\langle dT(z)/dz \rangle$ [Eq. (4)] are obtained. The number of time steps is 10^6 MD and their length $\Delta t = 1.0$ fs. The heat conductivity of the UA model is 0.26 ± 0.02 W m^{-1} K^{-1}, 0.25 ± 0.03 W m^{-1} K^{-1}, and 0.28 ± 0.03 W m^{-1} K^{-1} for cases I, II, and III, respectively. The thermal conductivities obtained by the two methods are, thus, consistent with each other. Moreover, the results obtained with the HI method at the three different heating rates agree within their statistical error. The findings indicate that the thermal conductivity calculated by classical MD simulation strongly depends on the number of degrees of freedom of the system. This is discussed in detail in Ref. [8].

In summary, we have developed two nonequilibrium simulation methods termed the DT method and the HI method, which are both suitable for the calculation of thermal conductivities with good accuracy. They are based on simple algorithms, and it will be very easy to extend their range of application. In particular, there are no restrictions (e.g., force field) on the types of systems, including models with bond constraints. Especially, the DT method is preferable because it is much easier to set the average temperature of the system by selecting the temperatures of the two thermostated slabs (T_H and T_C) symmetric around the desired average temperature. It will be of great interest to incorporate

other widely used thermostats [13–15], instead of the Berendsen thermostat, with the simulation methods described in this paper.

One of the authors (T.T.) acknowledges the Research Center for Computational Science, Okazaki, Japan, for the use of their facilities. This work was supported by the "Schwerpunktprogramm 1155: Molecular Simulation in Chemical Engineering" of the Deutsche Forschungsgemeinschaft.

[1] W. G. Hoover, *Molecular Dynamics*, Lecture Notes in Physics Vol. 258 (Springer-Verlag, Berlin, 1986).
[2] F. Müller-Plathe, J. Chem. Phys. **106**, 6082 (1997).
[3] P. Bordat and F. Müller-Plathe, J. Chem. Phys. **116**, 3362 (2002).
[4] F. Müller-Plathe and P. Bordat, in *Novel Methods in Soft Matter Simulations*, edited by M. Karttunen, I. Vattulainen, and A. Lukkarinen, Lecture Notes in Physics Vol. 640 (Springer, Heidelberg, Germany, 2004).
[5] M. Zhang, E. Lussetti, L. E. S. de Souza, and F. Müller-Plathe, J. Phys. Chem. B **109**, 15060 (2005).
[6] F. Müller-Plathe, Comput. Phys. Commun. **78**, 77 (1993).
[7] T. Terao and F. Müller-Plathe, J. Chem. Phys. **122**, 081103 (2005); **123**, 217101 (2005).
[8] E. Lussetti, T. Terao, and F. Müller-Plathe (unpublished).
[9] M. P. Allen and D. J. Tildesley, *Computer Simulation of Liquids* (Oxford University Press, Oxford, 1987).
[10] S. Goudeau, M. Chalot, C. Vergalati, and F. Müller-Plathe, Macromolecules **37**, 8072 (2004).
[11] D. J. Evans and G. P. Morris, *Statistical Mechanics of Nonequilibrium Liquids* (Academic Press, San Diego, 1990).
[12] F. Müller-Plathe and D. Brown, Comput. Phys. Commun. **64**, 7 (1991).
[13] For example, C. P. Lowe, Europhys. Lett. **47**, 145 (1999).
[14] S. Nosé, J. Chem. Phys. **81**, 511 (1984).
[15] W. G. Hoover, Phys. Rev. A **31**, 1695 (1985).